The importance of holes in aluminium tris-8-hydroxyquinoline (Alq3) devices with Fe and NiFe contacts

Hongtao Zhang, P. Desai, Y. Q. Zhan, A. J. Drew, W. P. Gillin, and T. Kreouzis

Citation: Applied Physics Letters **104**, 013303 (2014); doi: 10.1063/1.4861120
View online: http://dx.doi.org/10.1063/1.4861120
View Table of Contents: http://scitation.aip.org/content/aip/journal/apl/104/1?ver=pdfcov
Published by the AIP Publishing

The importance of holes in aluminium tris-8-hydroxyquinoline (Alq_3) devices with Fe and NiFe contacts

Hongtao Zhang,[1] P. Desai,[1] Y. Q. Zhan,[1,2] A. J. Drew,[1,3] W. P. Gillin,[1,2,3] and T. Kreouzis[1]
[1]*Materials Research Institute, School of Physics and Astronomy, Queen Mary University of London, Mile End Road, London E1 4NS, United Kingdom*
[2]*State Key Laboratory of ASIC and System, Department of Microelectronics, SIST, Fudan University, Shanghai 200433, China*
[3]*College of Physical Science and Technology, Sichuan University, Chengdu 610064, China*

(Received 1 October 2013; accepted 18 December 2013; published online 6 January 2014)

To study the dominant charge carrier polarity in aluminium tris-8-hydroxyquinoline (Alq_3) based spin valves, single Alq_3 layer devices with NiFe, ITO, Fe, and aluminium electrodes were fabricated and characterised by Time of Flight (ToF) and Dark Injection (DI) techniques, yielding a lower hole mobility compared to electron mobility. We compare the mobility measured by DI for the dominant carrier injected from NiFe and Fe electrodes into Alq_3, to that of holes measured by ToF. This comparison leads us to conclude that the dominant charge carriers in Alq_3 based spin valves with NiFe or Fe electrodes are holes. © *2014 AIP Publishing LLC*. [http://dx.doi.org/10.1063/1.4861120]

Over the last few decades, a considerable amount of research has been carried out on the archetypal organic semiconductor (OSC) aluminium tris-8-hydroxyquinoline (Alq_3), as it is used in both organic light emitting diode (OLED) and organic spin valve (OSV) fabrication.[1,2] OSVs and OLEDs share many similarities in structure and fabrication techniques, although they differ in, for example, operational parameters such as the applied bias.[3,4] Both rely on the injection of holes from the anode into the highest occupied molecular orbital (HOMO) and/or the injection of electrons from the cathode into the lowest unoccupied molecular orbital (LUMO) of the organic material. Since the operation of OSVs rely on the spin polarised injection and extraction of at least one type of carrier, it is of paramount importance to study the injection of charges from ferromagnetic (FM) electrodes. Since Alq_3 is widely used as an electron transport material it has been assumed that electrons are the dominant charge carrier in OSVs.[4–8] In addition to the charge carrier mobility, however, one must consider *carrier injection*, that is, the alignment between the Fermi levels of the electrodes and the HOMO and LUMO of the OSC.[9] For OSVs, the magnetic contacts are normally based on either $La_{0.67}Sr_{0.33}MnO_3$ (LSMO) or transition metal electrodes, such as NiFe or FeCo.[10,11] Magnetic electrodes employed in OSVs, especially those involving transition metals, have high work functions, which generally preclude electron injection, but vacuum level shifts may improve the energy level alignment.[12] In this work, Time of Flight (ToF) and Dark Injection (DI) were used to investigate the mobility of both carrier types in Alq_3 and the dominant carriers injected from ITO and the ferromagnetic electrodes Fe and NiFe into Alq_3.

Alq_3 was purified using vacuum sublimation ($\sim 10^{-6}$ mbar pressure) prior to deposition. Metal and organic layers were vacuum deposited (using typical deposition pressures of 10^{-7}–10^{-6} mbar, at rates of 0.1 nm · s^{-1} to 0.5 nm · s^{-1}). Thickness measurements of the resulting layers were carried out using a Dektak surface profilometer.

A frequency-tripled (355 nm wavelength), pulsed (6 ns duration, with a typical energy density of 140 mJ · cm^{-2}), Big Sky Nd:YAG laser was used to generate carriers for ToF measurements during the application of a DC electric field. DI measurements were carried out using a TTi (TG5011) pulse generator and a Trek Model 609E-6 high-voltage power amplifier. For both DI and ToF, the current through the device was monitored as a function of time as the voltage drop across a load resistor using an Agilent Infiniium digitising oscilloscope. The measured sample capacitance was typically in the range of $0.1 \sim 0.3$ nF. The choice of resistor ensured that the electronic RC time constant remained at least 10 times shorter than the carrier transit time. For the spin-valve, magnetoresistance was measured by a Cryogenic Limited-Cryogen Free Measurement System at 50 K under a 10–20 mbar Helium atmosphere and its IV characteristic measured using a Keithley 2612A source-measure unit.

ToF was used to perform direct measurements of the electron and hole transport in Alq_3. In order to minimise the dark current through the sample, the bias was always applied in reverse polarity (e.g., Al biased positively) and differentiating between carrier polarities was achieved by the choice of illuminated electrode. Typical hole and electron photocurrent transients obtained from an ITO-Alq_3 (1.2 μm)-Al device are shown in Figures 1(a) and 1(b), respectively, both with varying bias (electric field). In both cases, we observe typical dispersive photocurrents where the fastest arrival time, t_0, is denoted by a sharp inflection point in the trace. The pre and post arrival time gradients of the double logarithmic plots are in agreement with the theoretical forms expected for dispersive transport. If one approximates the photocurrent, $I(t)$, to a power law over the pre and post arrival times these are

$$I(t) \propto t^{-(1-\alpha_1)} \text{ for } t < t_0 \quad \text{and} \quad I(t) \propto t^{-(1+\alpha_2)} \text{ for } t > t_0. \tag{1}$$

The arrival time itself scales as expected with increasing electric field in both cases, e.g., the hole arrival time is reduced from ~10 ms at 18 V bias for holes to ~2 ms at 83 V bias and similarly for the electrons the arrival time is reduced

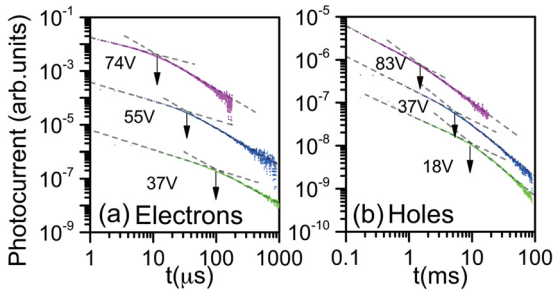

FIG. 1. Typical ToF photocurrent transients obtained from an ITO-Alq_3 (1.2 μm)-Al device. (a) Electron photocurrent transients with varying bias. (b) Hole photocurrent transients with varying bias. The transit time is indicated by an arrow for each photocurrent.

from $\sim$100 μs at 37 V bias to $\sim$10 μs at 74 V bias. The hole and electron mobilities obtained by ToF from various devices are shown as a Poole-Frenkel plot in Figure 2 in order to accommodate field dependent mobility. In our data, we have calculated the carrier mobility, μ, at a given field using

$$\mu = \frac{d^2}{Vt_t}, \tag{2}$$

where d is the sample thickness, V is the applied bias, and t_t is the transit time (t_0). The hole mobilities obtained from our samples are approximately two orders of magnitude lower than the electron mobilities. This is in qualitative agreement with the literature findings of the relative size of the electron and hole mobilities (also plotted in Figure 2) in this material using either ToF or Transient Electroluminescense (TEL).[13–19]

The ToF results, however, do not give us information on the mobility of the charge *injected* from the electrodes, merely the mobility of the carriers selected by the direction of the electric field within the sample. Using the same structure as the device in Figure 1, but using a thinner OSC layer (500 nm Alq_3), we obtained DI current transients, where samples were biased in the forward direction assuming the ITO is the anode and Al the cathode, to investigate *injected* charge. As there is no choice of illuminated electrode, one cannot differentiate between hole (injected from the ITO) and electron (injected from the aluminium) currents. The

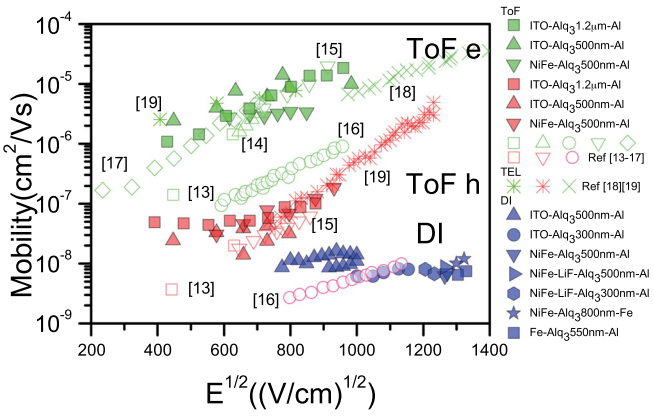

FIG. 2. Room temperature electron (green symbols) and hole (red symbols) mobility plotted versus the square root of electric field as measured by ToF, DI (blue symbols), and TEL in a variety of Alq_3 samples (including literature data, Refs. 13–19). The filled symbols are our data and the open symbols are taken from the literature.

shape of the transient response of the sample and any mobility calculated from it, however, will be determined by the carrier that is injected most efficiently.

Figure 3(a) shows typical DI transients obtained from ITO-Alq_3 (500 nm)-Al device. The initial current "spike" is due to the RC displacement current through the circuit (where $RC < 5$ μs). The current transients show a rise to a peak, followed by a reduction to the steady state space charge limited current (SCLC) value, as expected from the measurement. The time at which the peak occurs, t_{DI}, is related to the transit time, t_t, across the sample by $t_{DI} \sim 0.79t_t$ and we see that it scales correctly with increasing bias.[20,21] The DI results obtained from ITO-Alq_3 (500 nm)-Al devices demonstrate that carriers can both be injected in sufficient numbers and traverse the Alq_3 sample using conventional electrode materials. The mobility of these carriers is consistent with them being holes injected from the ITO anode.

In Alq_3 based OSVs, however, the devices with the highest magnetoresistance response utilise LMSO and Co as the contacts, not conventional electrode materials.[22] In addition, the current-voltage characteristics of a large number of OSVs are symmetric with the direction of applied bias, regardless of the contact combinations used, which have included: Fe-Alq_3-Co,[23] FeCo-P3HT-NiFe,[24] Co-Alq_3-Fe,[5]

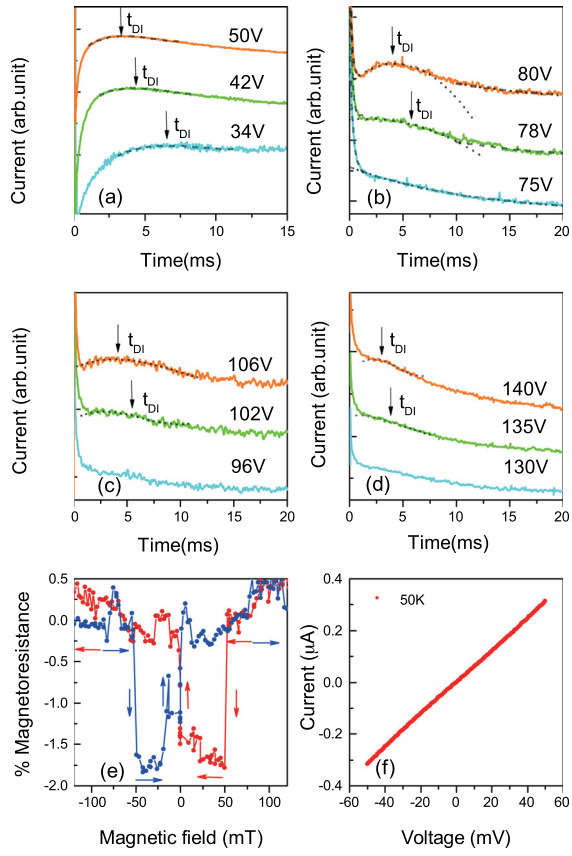

FIG. 3. (a) Typical DI currents obtained from an ITO-Alq_3(500 nm)-Al device showing the expected scaling of t_{DI} with bias. (b) Typical DI currents obtained from a NiFe-Alq_3(500 nm)-Al device displaying trapping decays as well as t_{DI}. (c) Typical DI currents obtained from a Fe-Alq_3(550 nm)-Al device displaying trapping decays as well as t_{DI}. (d) Typical DI currents obtained from a NiFe-Alq_3(800 nm)-Fe spin valve structure displaying trapping decays as well as t_{DI}. (e) Magnetoresistance obtained under 30 mV bias from a NiFe-Alq_3(100 nm)-Fe spin valve at 50 K. (f) Symmetric IV characteristic of a NiFe-Alq_3(100 nm)-Fe spin valve at 50 K.

NiFe-Alq_3-Co,[11] Co-AlO_x-Alq_3-Co,[6] LSMO-rubrene-Fe,[7] LSMO-Alq_3-Co,[25] LSMO-Alq_3-Co,[2,26] and Co-Ca-Alq_3-Ca-NiFe.[27] This shows that there is no rectification in any of these devices and hence the carriers injected from both contacts are the same. The symmetric characteristics of OSVs, including ones utilising Fe and NiFe electrodes, imply it is only necessary to determine the carrier type injected from one of the ferromagnetic contacts used in order to determine the carrier responsible for device operation. Figure 3(f) confirms the symmetric IV characteristics of the NiFe-Alq_3-Fe structures presented in this work. In order to demonstrate that both contacts give the same injected carrier type, we also studied devices with either NiFe and Al or Fe and Al contacts.

Figure 3(b) shows DI transients obtained using a NiFe-Alq_3 (500 nm)-Al device in forward bias, i.e., hole injection from the NiFe consistent with that observed for the ITO-Alq_3 (500 nm)-Al device presented in Figure 3(a). The peak required to define t_{DI} only becomes evident at very high bias, consistent with the extraction time becoming shorter than the trapping time, as expected. It is worth noting that no such transient response was obtained in reverse bias, with the only response being the RC displacement current. This means that there is no electron injection from the NiFe contact or hole injection from the aluminium. We can extract carrier mobility from forward bias traces, albeit over a very limited range, as the devices become unstable at high bias. Importantly, at all values of bias shown there is a long time-decay (two orders of magnitude larger than the RC time constant) in the current, which is typical of charge trapping within the sample.[28] Carrier trapping can be approximated by two sets of traps with typical trapping times of 0.24 ms and 45 ms. Figure 3(c) shows the DI response from an Fe-Alq_3(550 nm)-Al device, where the Fe is acting as the anode. Again it can be seen that the mobility is consistent with hole injection from the Fe anode.

Figure 3(d) shows both trapping and the presence of a t_{DI} extraction peak in an actual NiFe-Alq_3(800 nm)-Fe spin valve structure with the NiFe acting as the anode. The similarity between Figures 3(b) and 3(c) confirm that carrier injection into Alq_3 does not depend on the cathode used. We note that the Fe acts as a cathode in the NiFe-Alq_3(800 nm)-Fe device, in the configuration shown, yet the injected carrier mobility measured corresponds to holes in Alq_3. Figure 3(e) shows clear spin valve effect (Magnetoresistance) in a device constructed using the same electrode materials, albeit with a thinner Alq_3 layer. We note that there exist many examples of OSV structures utilising Alq_3 as the OSC, displaying both negative, as shown in Figure 3(e), as well as positive magnetoresistance.[29] Given that magnetoresistance is sensitive to interfacial injection layers[11] and to the overall device architecture[4] (electrode materials, OSC thickness, etc.), the sign of the magnetoresistance in our device, and its comparison to the literature goes beyond the scope of this article.

Mobilities obtained by DI in the four devices shown in Figure 3 were calculated using Eq. (2) and the relationship $t_t = t_{DI}/0.79$, and plotted in Figure 2. ToF measurements were also made on the thin (NiFe/ITO-Alq_3 (500 nm)-Al) devices used in DI. Due to the large absorption depth (~200 nm) in Alq_3 at the 355 nm laser wavelength used, these devices are ostensibly unsuitable for ToF. We have therefore plotted nominal calculated mobilities,[30] using an effective device thickness for charge transport of 500–200 = 300 nm, to demonstrate the consistency of these results with the ToF data obtained in 1.2 μm devices. The carrier mobilities obtained by DI are 2 to 3 orders of magnitude lower than the electron mobility measured by ToF in the same sample. However, the DI mobility is within a factor of 2 of the hole mobility obtained by ToF at the low electric fields which are closer to those utilised in OSV devices.

The small discrepancy between the DI mobility and the TOF hole mobility can be explained by a number of factors. A major difference between the ToF and DI measurements is that in DI the sample is "forward" biased and one possible explanation for the discrepancy in the mobility is that the electric field in the bulk of the sample in the DI measurements does not correspond to the applied bias divided by the sample thickness. This would be the case if there were significant voltage drops at the interfaces, resulting from charge accumulation (for example, due to interfacial traps). If this were the case, the calculated electric field in Figure 2 is overestimated for DI data and these mobilities are most likely to correspond to the low hole mobilities measured at small electric fields. Another possible explanation for the discrepancy between ToF and DI measured mobilities could lie in the dispersive nature of the charge transport, that is in the absence of a constant current plateau (see Figure 1). Whereas ToF measures an upper limit on the mobility (t_0 corresponds to the arrival time of the *fastest* carrier), DI measures an average mobility (t_{DI} is related to the average drift velocity).

Examining Figure 2, it becomes apparent that there is significant variation in hole and electron mobility measured in Alq_3 by various groups. In order to make this study meaningful, we have measured the hole and electron mobility by ToF in thick samples and compared this to a *nominal* mobility measured by ToF in same samples used for the DI measurements, although these were significantly thinner. Since the hole mobilities measured in both thick and thin samples, by our group, are comparable, we are confident that there is no significant sample to sample variation, including between thick and thin samples. This applies to thin samples utilising both FM and non-magnetic anodes. The DI mobilities obtained for the dominant carrier correspond to average mobilities (by virtue of the technique), display no significant field dependence or variation with layer thickness or anode material (ITO, Fe or NiFe) and do not depend on the cathode material. Even introducing a LiF interfacial layer at the NiFe electrode, which has been demonstrated to change the sign of the MR response in an Alq_3 based OSV device[11] had no effect on the carrier mobility measured by DI. The average carrier mobilities obtained by DI are of order 10^{-8} $cm^2V^{-1}s^{-1}$ and these compare closely to the upper limit hole mobilities (obtained by ToF) of order 5×10^{-8} $cm^2V^{-1}s^{-1}$ and extremely unfavourably with the electron mobilities (obtained by ToF) of order 5×10^{-6} $cm^2V^{-1}s^{-1}$. The DI mobilities of order 10^{-8} $cm^2V^{-1}s^{-1}$ correspond to the majority injected charge when NiFe and Fe act as the anode in the devices measured. Given this and the large work functions of both Fe and NiFe, we conclude that the

dominant carriers injected from Fe and NiFe into Alq_3 are holes and not electrons.

The authors gratefully acknowledge funding from the EU FP7 Project No. NMP3-SL-2011-263104 "HINTS," the Chinese Scholarship Council, the Royal Academy of Engineering and the Engineering and Physical Sciences Research Council (Grant No. EP/G054568/1).

[1]C. W. Tang and S. A. VanSlyke, Appl. Phys. Lett. **51**(12), 913 (1987).
[2]Z. H. Xiong, D. Wu, Z. V. Vardeny, and J. Shi, Nature **427**(6977), 821 (2004).
[3]N. Rolfe, P. Desai, P. Shakya, T. Kreouzis, and W. P. Gillin, J. Appl. Phys. **104**(8), 083703 (2008).
[4]V. A. Dediu, L. E. Hueso, I. Bergenti, and C. Taliani, Nature Mater. **8**(9), 707 (2009).
[5]Y. Liu, S. M. Watson, T. Lee, J. M. Gorham, H. E. Katz, J. A. Borchers, H. D. Fairbrother, and D. H. Reich, Phys. Rev. B **79**(7), 075312 (2009).
[6]X. Zhang, S. Mizukami, T. Kubota, M. Oogane, H. Naganuma, Y. Ando, and T. Miyazaki, IEEE Trans. Magn. **47**(10), 2649 (2011).
[7]J.-W. Yoo, H. W. Jang, V. N. Prigodin, C. Kao, C. B. Eom, and A. J. Epstein, Phys. Rev. B **80**(20), 205207 (2009).
[8]V. Dediu, L. E. Hueso, I. Bergenti, A. Riminucci, F. Borgatti, P. Graziosi, C. Newby, F. Casoli, M. P. De Jong, C. Taliani, and Y. Zhan, Phys. Rev. B **78**(11), 115203 (2008).
[9]K. Seki, E. Ito, and H. Ishii, Synth. Met. **91**(1), 137 (1997).
[10]M. Bowen, M. Bibes, A. Barthelemy, J.-P. Contour, A. Anane, Y. Lemaitre, and A. Fert, Appl. Phys. Lett. **82**(2), 233 (2003).
[11]L. Schulz, L. Nuccio, M. Willis, P. Desai, P. Shakya, T. Kreouzis, V. K. Malik, C. Bernhard, F. L. Pratt, N. A. Morley, A. Suter, G. J. Nieuwenhuys, T. Prokscha, E. Morenzoni, W. P. Gillin, and A. J. Drew, Nature Mater. **10**(1), 39 (2011).
[12]Y. Q. Zhan, M. P. de Jong, F. H. Li, V. Dediu, M. Fahlman, and W. R. Salaneck, Phys. Rev. B **78**(4), 045208 (2008).
[13]R. G. Kepler, P. M. Beeson, S. J. Jacobs, R. A. Anderson, M. B. Sinclair, V. S. Valencia, and P. A. Cahill, Appl. Phys. Lett. **66**(26), 3618 (1995).
[14]T. Tsutsui, H. Tokuhisa, and M. Era, "Polymer photonic devices," Proc. SPIE **3281**, 230 (1998).
[15]S. Naka, H. Okada, H. Onnagawa, Y. Yamaguchi, and T. Tsutsui, Synth. Met. **111**, 331 (2000).
[16]H. H. Fong and S. K. So, J. Appl. Phys. **100**(9), 094502 (2006).
[17]R. L. Martin, J. D. Kress, I. H. Campbell, and D. L. Smith, Phys. Rev. B **61**(23), 15804 (2000).
[18]H. Park, D.-S. Shin, H.-S. Yu, and H.-B. Chae, Appl. Phys. Lett. **90**(20), 202103 (2007).
[19]A. G. Mückl, S. Berleb, W. Brütting, and M. Schwoerer, Synth. Met. **111–112**(0), 91 (2000).
[20]J. Y. Song, N. Stingelin, W. P. Gillin, and T. Kreouzis, Appl. Phys. Lett. **93**(23), 233306 (2008).
[21]M. A. Lampert and P. Mark, *Current Injection in Solids* (Academic Press, New York, 1970).
[22]C. Barraud, P. Seneor, R. Mattana, S. Fusil, K. Bouzehouane, C. Deranlot, P. Graziosi, L. Hueso, I. Bergenti, and V. Dediu, Nat. Phys. **6**(8), 615 (2010).
[23]F. J. Wang, Z. H. Xiong, D. Wu, J. Shi, and Z. V. Vardeny, Synth. Met. **155**(1), 172 (2005).
[24]N. A. Morley, A. Rao, D. Dhandapani, M. R. J. Gibbs, M. Grell, and T. Richardson, J. Appl. Phys. **103**(7), 07F306 (2008).
[25]S. Wang, Y. J. Shi, L. Lin, B. B. Chen, F. J. Yue, J. Du, H. F. Ding, F. M. Zhang, and D. Wu, Synth. Met. **161**(15–16), 1738 (2011).
[26]D. Sun, L. Yin, C. Sun, H. Guo, Z. Gai, X.-G. Zhang, T. Z. Ward, Z. Cheng, and J. Shen, Phys. Rev. Lett. **104**(23), 236602 (2010).
[27]H.-J. Jang, K. P. Pernstich, D. J. Gundlach, O. D. Jurchescu, and C. A. Richter, Appl. Phys. Lett. **101**(10), 102412 (2012).
[28]A. Many and G. Rakavy, Phys. Rev. **126**(6), 1980 (1962).
[29]T. S. Santos, J. S.Lee, P. Migdal, I. C. Lekshmi, B. Sapati, and J. S. Moodera, Phys. Rev. Lett. **98**(1), 016601 (2007).
[30]D. Z. Garbuzov, V. Bulović, P. E. Burrows, and S. R. Forrest, Chem. Phys. Lett. **249**(5–6), 433 (1996).